buildings

MDPI

Article

Shear Bearing Capacity Prediction of Steel-Fiber-Reinforced High-Strength Concrete Corbels on Modified Compression Field Theory

Hong-Mei Li [1,2], Jin-Yan Zheng [1,*] and Shu-Shan Li [1,2]

[1] School of Civil Engineering and Communication, North China University of Water Resources and Electric Power, Zhengzhou 450046, China; lihongmei@ncwu.edu.cn (H.-M.L.); lishushan@ncwu.edu.cn (S.-S.L.)
[2] Engineering Technology Research Center for Structural Vibration Control and Health Monitoring of Henan Province, Zhengzhou 450046, China
* Correspondence: zhengjinyan@stu.ncwu.edu.cn; Tel.: +86-187-4916-5371

Abstract: In order to analyze the shear mechanism of the steel-fiber high-strength concrete corbels, a calculation model for the shear bearing capacity of steel-fiber-reinforced high-strength concrete corbels was proposed based on the modified compression field theory. Considering the existence of residual tensile stress in steel-fiber-reinforced concrete at crack locations, the cracked steel-fiber-reinforced concrete was treated as a continuous material. The constitutive relation of cracked steel-fiber-reinforced concrete and the local stress equilibrium equation were modified. It was compared with the results of 34 steel-fiber high-strength concrete corbels, including those in this paper. The predicted results were compared with the experimental values and the predictions of the Fattuhi model, Campione model, and Russo model to validate the rationality of the proposed model. The results revealed that the mean value between the experimental values and the predicted results of the proposed model is 1.104, with a variance of 0.003, showing good agreement. The proposed model can accurately predict the shear bearing capacity of steel-fiber-reinforced high-strength concrete corbels.

Keywords: corbel; local stress; modified compression field theory; steel-fiber-reinforced high-strength concrete; shear bearing capacity

check for updates

Citation: Li, H.-M.; Zheng, J.-Y.; Li, S.-S. Shear Bearing Capacity Prediction of Steel-Fiber-Reinforced High-Strength Concrete Corbels on Modified Compression Field Theory. *Buildings* **2024**, *14*, 388. https://doi.org/10.3390/buildings14020388

Academic Editor: Grzegorz Ludwik Golewski

Received: 9 December 2023
Revised: 16 January 2024
Accepted: 19 January 2024
Published: 1 February 2024

Copyright: © 2024 by the authors. Licensee MDPI, Basel, Switzerland. This article is an open access article distributed under the terms and conditions of the Creative Commons Attribution (CC BY) license (https://creativecommons.org/licenses/by/4.0/).

1. Introduction

As cantilever support structures, reinforced concrete corbels are important vertical load-bearing components in practical engineering applications such as industrial plants and road bridges. The steel-fiber-reinforced high-strength concrete formed by incorporating steel fibers into high-strength concrete is a type of composite material that not only overcomes the drawbacks of poor ductility and brittleness of high-strength concrete [1,2], but it also enhances the cracking, tensile, and shear strength of concrete. The application in the corbels can effectively improve the shear performance and bearing capacity of the structure [3–5].

The internal stress state of corbels becomes complex under the action of loads, the presence of non-linear strain behavior, and significant stress redistribution across the section. They belong to the category of typical D-region members [6]. According to Saint-Venant's principle [7], the D-region has the characteristics of discontinuity in a geometric structure or disturbances in the flow of forces, which are no longer suitable for design theory assumed by the plane section [8,9]. Khattab et al. [10] conducted experimental research on the corbels with different shear span ratios, and compared the test results with those calculated using the shear friction and strut-and-tie models specified in ACI 318-14 [11]. Malgorzata et al. [12] performed experiments on reinforced concrete corbels. By fitting and analyzing the test results, the formula for calculating the inclined crack of the corbels is proposed. Yang et al. [13] proposed a calculation method for predicting the shear

carrying capacity of reinforced concrete corbels, which showed better predictive results compared to other existing models. Wael et al. [14] presented a reinforced concrete corbel bearing capacity calculation method based on the strut-and-tie model. The results indicated that the proposed strut-and-tie method provided sufficiently accurate predictions, leading to the conclusion that it offers safe and reliable approach for calculating the bearing capacity of corbels. Perceka et al. [15] made 10 high-strength steel-fiber concrete beams. Based on the observation results of the test results and the evaluation results of the previous shear strength equations, the prediction equation of the shear strength of steel-fiber concrete beams was proposed. Muhammad et al. [16] conducted pouring tests on 12 BFRP-reinforced concrete beams. In addition, based on the published experimental shear strength and test results of 217 FRP-RC beams without stirrup, the equation for predicting the contribution of concrete to the shear strength of FRP-RC beams was established with good accuracy. However, there is a limited amount of reported research on the calculation models and methods specifically used for steel-fiber-reinforced high-strength concrete corbels, and there is no unified calculation model and method for the calculation of its bearing capacity, which cannot meet the needs of practical engineering design. In 1986, Canadian scholars Vecchio and Collins [17] proposed the modified compression field theory (MCFT) based on the existing theory of the compression field, which considered the equilibrium, compatibility conditions, and the constitutive relationship of cracked concrete. MCFT has been widely recognized for the analysis of membrane, beam, plate, shell, and plane frames. Even the more complex structural analysis results are ideal, and it is also suitable for steel-fiber-reinforced concrete structures [18,19]. Gao et al. [20] and Zhang et al. [21], Zhu et al. [22], Lei et al. [23], used MCFT to study the shear capacity of reinforced steel-fiber concrete beam–column joints, steel-fiber high-strength concrete two-pile cap, and hybrid concrete deep beams, respectively. The results showed that the predicted shear strength is in good agreement with the experimental results. The modified pressure field theory takes into account the tensile stress of cracked concrete and determines the average stress, average strain, and crack angle according to the equilibrium conditions, compatibility conditions, and the stress–strain relationship between reinforced and cracked concrete. Finally, the shear bearing capacity of reinforced concrete members under the action of shear force can be obtained, which is more accurate and reasonable.

The current research proposes a model that calculates the shear bearing capacity of steel-fiber-reinforced high-strength concrete corbels based on MCFT. The proposed model considers the stress transfer of steel fiber as the crack corrects the constitutive relationship of steel-fiber-reinforced concrete, allowing for a better reflection of the shear behavior of steel-fiber-reinforced high-strength concrete corbels. It was used to predict the shear capacity of 31 specimens, including the specimens tested in this study. The predicted results were compared with the experimental results and simultaneously compared with calculation models proposed by other scholars to evaluate its accuracy.

2. Establishment of the Proposed Model

The modified compression field theory incorporates stress equilibrium conditions both between and within cracks, offering a comprehensive and practical theoretical framework, and includes the following aspects:

- The shear stress and normal stress experienced by concrete micro-elements are uniformly distributed when subjected to loads.
- The stress and strain of concrete refer to the average stress and strain in the cracking zone.
- The principal stress and principal strain directions of concrete are consistent.
- There is no bond slip between steel bars and concrete, assuming ideal bond conditions.
- Shear stress in steel bars is not considered: only the axial stress in the steel bars is taken into account.

2.1. Equilibrium Conditions

Assuming that the cracked steel-fiber-reinforced high-strength concrete is a homogeneous composite material (whereby Figure 1 illustrates Mohr's circle of average stress), the following relationships are determined:

$$f_x = f_1 - v\cot\theta + \rho_{sx} f_{sx} \tag{1}$$

$$f_y = f_1 - v\tan\theta \tag{2}$$

$$f_1 + f_2 = v(\tan\theta + \cot\theta) \tag{3}$$

where f_1 is the principal tensile stress of the concrete; f_2 is the principal compressive stress of the concrete; f_x and f_y are the average stresses of the element along the x and y directions, respectively; θ represents the inclination of the diagonal compressive; v is the shear stress by the element; f_{sx} is the stress in the x direction of the steel reinforcement; and ρ_{sx} is the reinforcement ratio in the x direction.

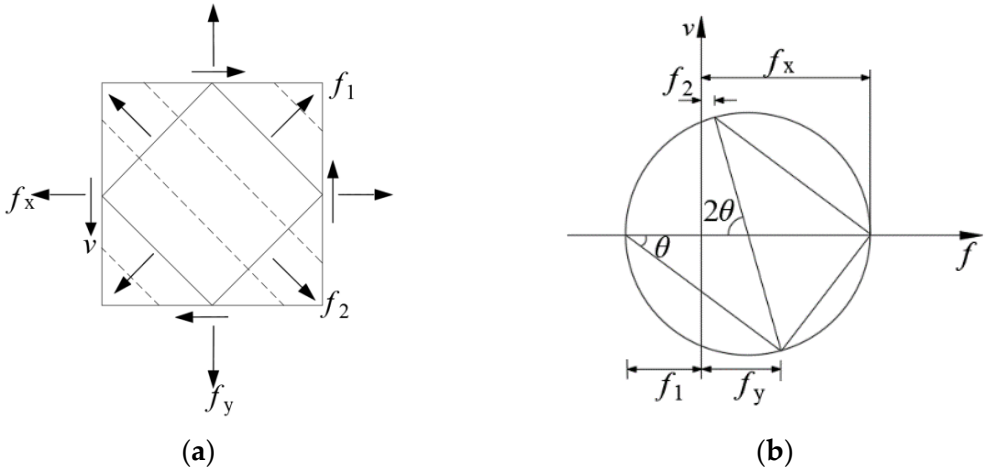


Figure 1. Average stress Mohr's circle of concrete. (**a**) Average stress of concrete; (**b**) Average stress Mohr's circle.

After cracking, steel-fiber concrete corbels continue to transmit stress across the cracks. The bond between concrete and steel fibers enhances the stress at the crack, providing a bridging effect. This effectively inhibits crack propagation and improves the transfer of shear forces across the crack interfaces [24]. Considering the steel of fibers on concrete shear resistance under the stress balance condition at the crack, the residual tensile stress generated by steel fiber is as follows:

$$\sigma_f = K_f \frac{L_f}{D_f} \tau_u \rho_f \tag{4}$$

where K_f is the effective distribution coefficient of steel fibers; L_f is the length of the steel fibers; D_f is the diameter of steel fibers; τ_u is the bond strength between steel fibers and concrete, whereby $\tau_u = 0.6 f_c'2/3$ [18]; and ρ_f represents the volume fraction of steel fibers.

Steel fibers are randomly distributed in the concrete matrix, and when the fiber pullout angle exceeds a certain limit, it is considered that the steel fibers have little contribution to the tensile strength of the concrete [25,26]. Therefore, assuming that the x-axis direction is the normal direction of the crack surface, the angle formed between a single steel fiber and the x-axis direction is θ_f, as shown in Figure 2.

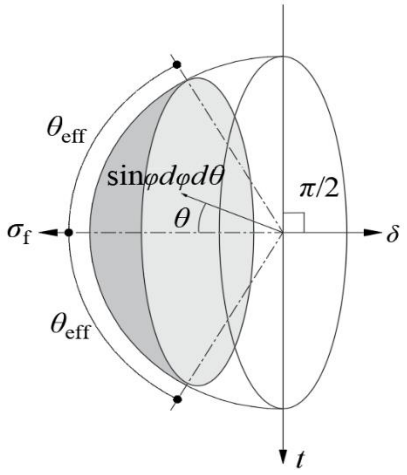


Figure 2. The effective orientation of the steel fiber.

According to Foster's research findings [27], when the fiber pullout angle exceeds 60 degrees, the contribution of steel fibers is not considered. The fiber inclination is between 0 and 60 degrees. The effective distribution coefficient of randomly oriented steel fibers in concrete is calculated by integrating according to the following equation:

$$K_f = \frac{1}{2\pi}\int_{-\pi}^{\pi}\int_{0}^{60^\circ} \cos\theta_f \sin\theta_f d\theta_f d\varphi \tag{5}$$

For the steel-fiber concrete corbels, the bridging effect of steel fibers enhances the shear stress. Thus, the balance of transverse reinforcement direction (x direction) force can be expressed as follows:

$$\rho_{sx} f_{sx} + f_1 \sin^2\theta - f_2 \cos^2\theta = 0 \tag{6}$$

Similarly, the balance of forces in the y direction is:

$$f_1 - v\tan\theta - \sigma_n = 0 \tag{7}$$

where σ_n is the axial compressive stress, which is taken as $\sigma_n = nf_c'$; n is the axial load ratio ($n = N/f_c'bh_0$; N is the axial load and b is the width of the corbel section).

From Equation (8), it can be expressed as:

$$f_1 bh_0 - V\tan\theta = N \tag{8}$$

2.2. Constitutive Relations

2.2.1. Stress–Strain Relationship of Concrete in Tension

The concrete is considered to be in the linear elastic stage before cracking, that is, the tensile stress–strain relationship is as follows:

$$f_1 = E_c\varepsilon_1 (\varepsilon_1 \le \varepsilon_{cr}) \tag{9}$$

where E_c is the elastic modulus of concrete; ε_1 is the principal tensile strain.

The tensile stress–strain relationship of cracked concrete is given by [28]:

$$f_1 = \frac{0.33\sqrt{f_c'}}{1+\sqrt{500\varepsilon_1}} (\varepsilon_1 > \varepsilon_{cr}) \tag{10}$$

where f_c' is the compressive strength of concrete cylinder; ε_{cr} is the cracking strain of concrete, given by $\varepsilon_{cr} = 0.33 f_c'^{(1/2)}/E_c$ [17].

For the principal tensile stress and strain relationship of steel fiber concrete, the reinforcement effect of steel fiber on concrete is considered. The tensile stress in cracked

steel-fiber-reinforced concrete is equal to the residual tensile stress in concrete plus the tensile stress in steel fibers at the crack location [29]. The expression is given by:

$$f_1 = \frac{0.33\sqrt{f'_c}}{1+\sqrt{500\varepsilon_1}} + \sigma_f(\varepsilon_1 > \varepsilon_{cr}) \tag{11}$$

2.2.2. Stress–Strain Relationship of Concrete in Compression

The stress–strain relationship of steel-fiber-reinforced concrete in compression, as suggested by Vecchio and Collins [30,31], is as follows:

$$f_2 = f_{2,max}\left[2\left(\frac{\varepsilon_2}{\varepsilon_0}\right) - \left(\frac{\varepsilon_2}{\varepsilon_0}\right)^2\right] \tag{12}$$

$$\frac{f_{2,max}}{f'_c} = \frac{1}{0.8 - 0.34\frac{\varepsilon_1}{\varepsilon_0}} \leq 1 \tag{13}$$

where $f_{2,max}$ is the maximum principal compressive stress in the concrete; ε_0 is the compressive strain of concrete corresponding to the maximum principal compressive stress, which is generally -0.002; ε_1 and ε_2 are the strains corresponding to the principal tensile stress and the principal compressive stress.

2.2.3. Stress–Strain Relationship of Reinforcement

The stress–strain relationship for steel in tension and compression is used by an ideal elastic–plastic model, which can be expressed as:

$$f_s = E_s\varepsilon_s \leq f_y \tag{14}$$

where f_s and ε_s represent the stress and strain of steel reinforcement, respectively; E_s denotes the steel reinforcement elastic modulus; and f_y represents the yield strength of the steel reinforcement.

2.3. Compatibility Conditions

Assuming no slippage between the steel reinforcement and concrete, the deformation amount of reinforcement and concrete is exactly the same. Therefore, the incremental strain values of the concrete and steel are also same. At the instant of cracking, the incremental strain and stress values of the steel reinforcement can be neglected, resulting in the following equation:

$$\varepsilon_{cx} = \varepsilon_{sx} = \varepsilon_x \tag{15}$$

$$\varepsilon_{cy} = \varepsilon_{sy} = \varepsilon_y \tag{16}$$

where ε_{cx} and ε_{cy} are the concrete strain in x and y directions, respectively; ε_{sx} and ε_{sy} are the strain in the x and y directions of the reinforcement, respectively; ε_x and ε_y are the strains in the x and y directions of the element.

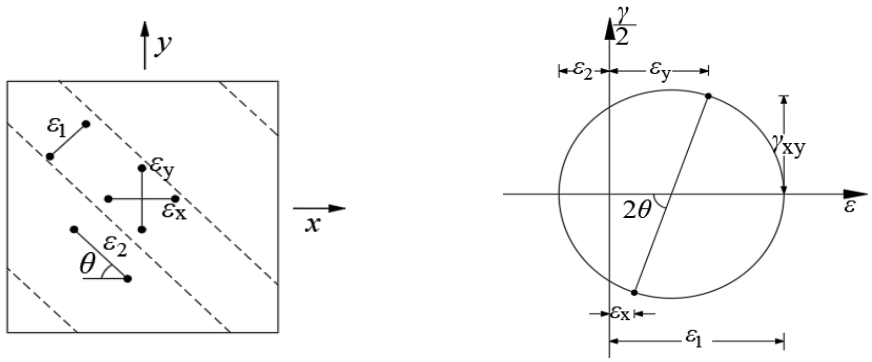
The geometric relationship between the principal strains of concrete and Mohr's circle of average strain (Figure 3) is given as follows:

$$\tan 2\theta = \frac{\gamma_{xy}}{\varepsilon_y - \varepsilon_x} \tag{17}$$

$$\varepsilon_1 + \varepsilon_2 = \varepsilon_x + \varepsilon_y \tag{18}$$

$$\tan^2\theta = \frac{\varepsilon_x - \varepsilon_2}{\varepsilon_y - \varepsilon_2} = \frac{\varepsilon_1 - \varepsilon_y}{\varepsilon_y - \varepsilon_2} \tag{19}$$

where ε_1 and ε_2 are the principal tensile and compressive strains of the element, respectively, while γ_{xy} is the shear strain.



(**a**) (**b**)

Figure 3. Compatibility conditions for cracked concrete. (**a**) Average strain for cracked concrete; (**b**) Mohr's circle of average stress.

From (18)–(20), we can obtain:

$$\varepsilon_x = \varepsilon_1 \cos^2\theta + \varepsilon_2 \sin^2\theta \tag{20}$$

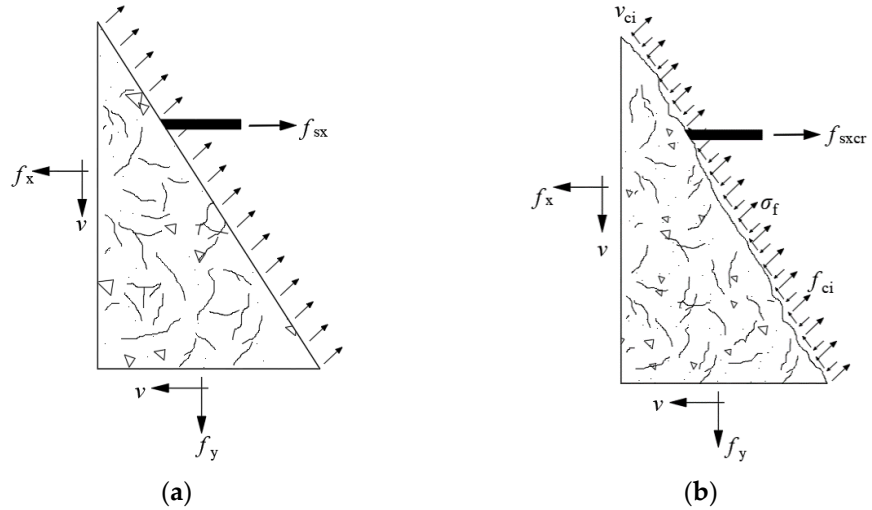
$$\varepsilon_y = \varepsilon_1 \sin^2\theta + \varepsilon_2 \cos^2\theta \tag{21}$$

$$\gamma_{xy} = 2(\varepsilon_1 - \varepsilon_2)\sin\theta\cos\theta \tag{22}$$

2.4. Stress Equilibrium of Steel Fibers at the Crack

In the MCFT, the average stress is assumed to be in equilibrium with the stress at the crack location using the static equivalence method. This allows for a reasonable simplification of the actual complex stress state, considering it as an ideal series of parallel cracks. Figure 4 shows the stress distribution of the cracked unit at the crack location and between cracks. Because the compressive stress f_{ci} at the crack is relatively small, its influence can be ignored. Considering the stress equilibrium in the direction of the stirrup, the following can be obtained:

$$\rho_{sx} f_{sx} \sin\theta + f_1 \sin\theta = \rho_{sx} f_{sxcr} \sin\theta - v_{ci} \cos\theta + \sigma_f \sin\theta \tag{23}$$



(**a**) (**b**)

Figure 4. Stress distribution at the crack and between cracks. (**a**) Average stress between cracks; (**b**) Local stress at cracks.

Thus,

$$f_1 = (\rho_{sx} f_{sxcr} - \rho_{sx} f_{sx}) - v_{ci} \cot\theta + \sigma_f \tag{24}$$

where f_{sxcr} is the reinforcement stress in the x direction of the crack, and v_{ci} is the shear stress at the crack, which can be calculated by the following formula:

$$v_{ci} = \frac{0.18\sqrt{f'_c}}{0.3+\frac{24w}{a+16}} \tag{25}$$

The size of the crack spacing mainly depends on the distribution of longitudinal steel bars and stirrups. The denser the arrangement of steel reinforcement, the closer the cracks, and the corresponding spacing decreases. The crack width can be calculated using the following equation:

$$w = \varepsilon_1 s_\theta \tag{26}$$

$$s_\theta = \frac{1}{\frac{\sin\theta}{s_{mx}} + \frac{\cos\theta}{s_{my}}} \tag{27}$$

where a is the maximum aggregate size, w is the crack width, s_θ is the average crack spacing, s_{mx} is the crack spacing in the x direction, and s_{my} represents the crack spacing in the y direction. To simplify, the maximum spacing between longitudinal reinforcement and stirrups is used in the above calculation.

When the reinforcement at the crack reaches its yield strength, the control condition for the principal tensile stress f_1 can be obtained via Equation (24):

$$f_1 \le \rho_{sx}(f_{sxy} - f_{sx}) - v_{ci}\cot\theta + \sigma_f \tag{28}$$

At the same time, the control condition for the reinforcement stress at the crack is given by:

$$f_{sxcr} = f_{sx} + (f_1 + v_{ci}\cot\theta - \sigma_f)/\rho_{sx} \le f_{sxy} \tag{29}$$

By combining Equations (3) and (6), we can obtain:

$$v = \rho_{sx} f_{sx}\tan\theta + (v_{ci}\tan\theta + \sigma_f)\tan\theta \tag{30}$$

The shear capacity of steel-fiber-reinforced high-strength concrete corbels is obtained via:

$$V = A_{sv} f_y \frac{h_0}{s}\tan\theta + (v_{ci}\tan\theta + \sigma_f) b h_0 \tan\theta \tag{31}$$

2.5. Calculation Process

The abovementioned equilibrium conditions, constitutive relations, compatibility conditions, and stress equilibrium of steel fibers at the crack are solved simultaneously to calculate the shear capacity of steel-fiber-reinforced high-strength concrete corbels. Figure 5 illustrates the flowchart of the solution process, which involves the following main steps:

1. Input corbels' geometry and material parameters.
2. Assume ε_1, and the increment of ε_1 is 0.0001.
3. Assume θ.
4. Calculate v_{ci} and w using Equations (25) and (26).
5. Assume f_{sx0}.
6. Calculate f_1 using Equation (11), and satisfy Equation (28).
7. Calculate v using Equation (30).
8. Calculate f_2 using Equation (3), and f_2 is limited by $f_{2,max}$.
9. Use Equation (14) to determine whether it is equal to the assumed f_{sx0}. If it is, continue to the next step; otherwise, return to (6) to assume the stirrup stress again.
10. Calculate axial load N using Equation (8), and whether the axial force is equal to 0. If it is true, the analysis of the corresponding principal tension strain state is completed. If not, return to (4) to assume the crack inclination again until it is equal.

11. Calculate f_{sxcr} using Equation (29), if f_{sxcr} is less than f_{sxy}, the calculation ends. Otherwise, return to (2) to re-assume the main tensile strain of concrete.

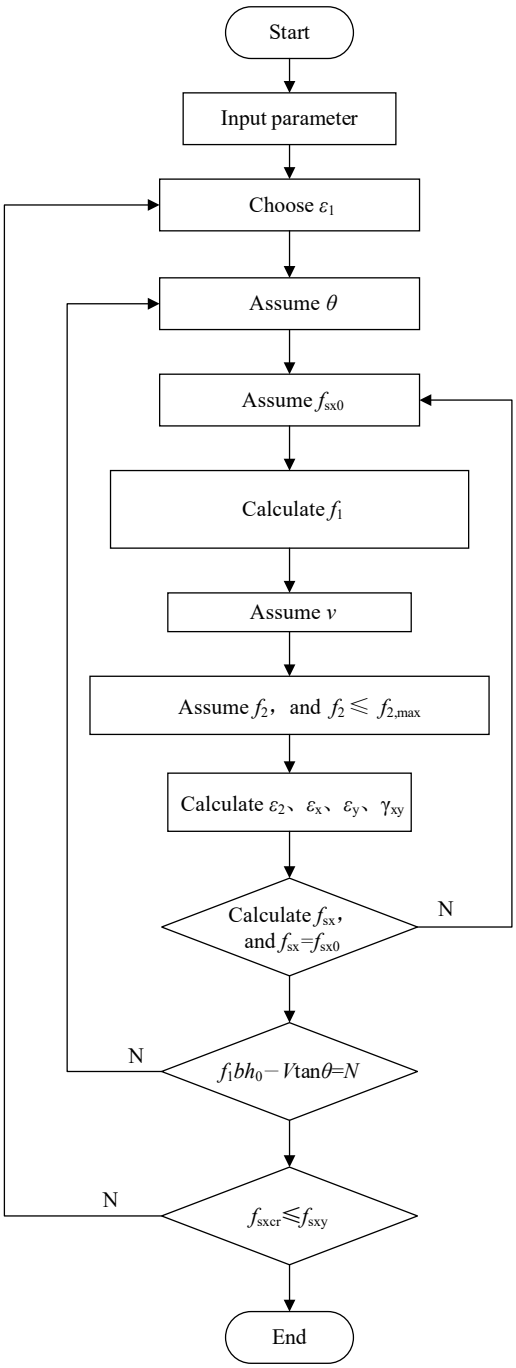


Figure 5. Calculation flow chart.

3. Model Verification

3.1. Experimental Work

With the aim of verifying the above shear bearing capacity calculation model, the shear test of nine steel-fiber high-strength concrete corbels under concentrated load was completed, with a width of 200 mm, a height of 450 mm at the root cross-section, and a width of 200 mm. The design parameters of the shear span-to-depth ratio (λ), the steel fiber dosage (ρ_f), the main reinforcement ratio (ρ_s), the stirrup reinforcement ratio (ρ_{sh}), and the main parameters and reinforcement are shown in Table 1 and Figure 6.

Table 1. Specimen parameters.

Specimens	Main Reinforcement	Ratio of Reinforcement	Stirrup	Stirrup Reinforcement Ratio	Shear Span Ratio	Effective Depth	Steel Fiber Dosage
MC01	4C12	0.55%	A10@100	0.785%	0.2	400	1.5%
MC02	4C12	0.55%	A10@100	0.785%	0.3	400	1.5%
MC03	4C12	0.55%	A10@100	0.785%	0.4	400	1.5%
MC04	4C12	0.55%	A10@100	0.785%	0.3	400	1.5%
MC05	4C12	0.55%	A10@100	0.785%	0.3	400	1.5%
MC06	4C12	0.75%	A10@150	0.390%	0.3	400	1.5%
MC07	4C12	0.98%	A10@200	0.520%	0.3	400	1.5%
MC08	4C12	0.55%	A10@100	0.785%	0.3	400	0
MC09	4C12	0.55%	A10@100	0.785%	0.3	400	0.75%

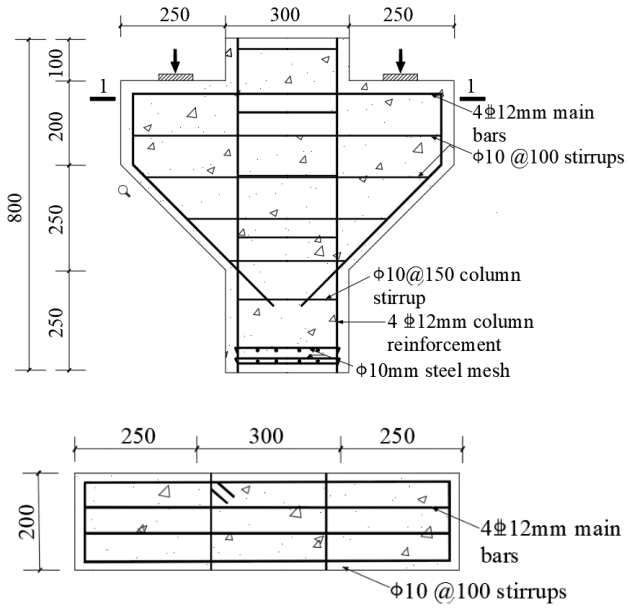


Figure 6. Specimen dimension and reinforcement.

The longitudinal reinforcement and stirrup reinforcement of the specimens were made of HRB400- and HPB300-grade steel bars, respectively. The measured mechanical properties of various types of steel reinforcement are presented in Table 2.

Table 2. Measured mechanical properties of reinforcement.

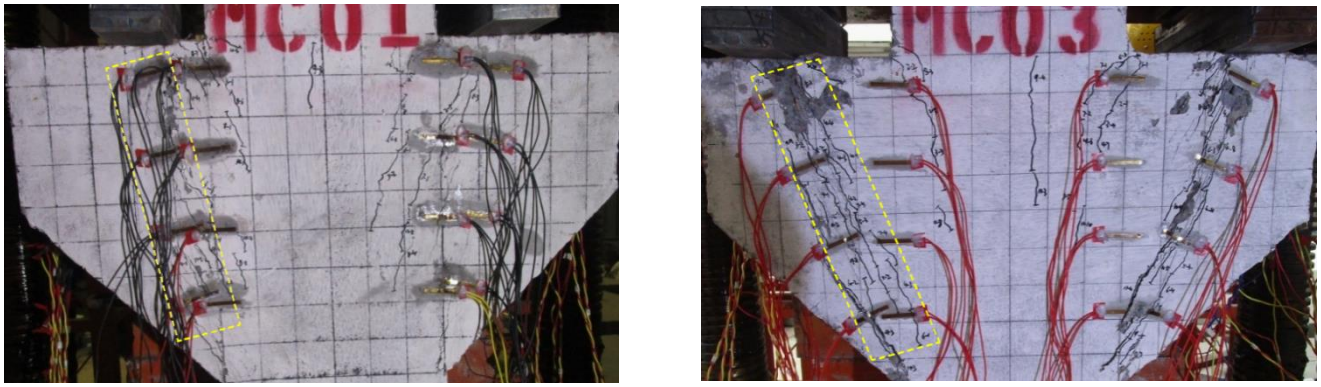
Reinforcement Type	Diameter (mm)	Cross-Sectional Area (mm^2)	Yield Strength (MPa)	Elastic Modulus (GPa)	Ultimate Strength (MPa)
HPB300	10	78.5	333.7	195.95	535.8
HRB400	12	113.1	425.2	172.6	541.4
HRB400	14	153.9	467.8	185.0	582.3
HRB400	16	201.1	427.3	192.5	587.7

The main test results and failure patterns of the specimens are shown in Table 3. All specimens experienced shear failure, and can be divided into three stages, namely initial cracking, critical cracking, and ultimate failure. Due to the difference in shear span ratio, the typical failure modes of the specimen include diagonal shear failure and diagonal compression failure. The top longitudinal tensile reinforcement gradually reaches the yield strength, and the penetrating diagonal crack appears at the connection surface between the loading plate and the column, forming the concrete failure mode caused by shear force.

As shown in Figure 7a, the failure section is close to the vertical and slightly oblique shear crack, which resulted in the patterns of diagonal shear failure. Figure 7b shows that the middle part of the diagonal direction is perpendicular to the direction of the main tensile stress, and several oblique ventral shear cracks that are roughly parallel to each other appear successively, and oblique prisms appear in the abdomen of the corbel. After the occurrence of the main oblique crack, when the ultimate load is approaching, the yield strength of the longitudinal tensile reinforcement part reaches the vertical part, which led to the patterns of diagonal compression failure.

Table 3. Test results and failure patterns of specimens.

Specimens	V_{cr}^{N}/kN	V_{cr}^{D}/kN	V_u/kN	Failure Patterns
MC01	270	400	879	Diagonal shear patterns
MC02	220	290	822	Diagonal compression pattern
MC03	166.5	255	695	Diagonal compression pattern
MC04	220	355	874	Diagonal compression pattern
MC05	193	386.5	981.5	Diagonal compression pattern
MC06	192	234.5	670.5	Diagonal compression pattern
MC07	164	240	751	Diagonal compression pattern
MC08	150	331	775	Diagonal compression pattern
MC09	180	381	767	Diagonal compression pattern



(**a**) (**b**)

Figure 7. Failure patterns of specimens: (**a**) specimen MC01; (**b**) specimen MC03.

3.2. Comparison with Test Results

A comparative analysis was conducted by selecting shear capacity models proposed based on the Fattuhi model [32], Campione model [33], and Russo model [34] and by comparing them with the model presented in this paper. The introduction is presented below.

3.2.1. Fattuhi Model [32]

The formulation takes into account the contributions of both traditional bar reinforcement and fibrous reinforcement, considering their respective volumes and their influence on the mechanical behavior of the corbels. Fattuhi proposed an empirical formulation based on experimental data:

$$V = k_1 bh(f_t)^{k_2}\left(\frac{f_y}{f_{cu}}\right)^{k_4}\left(\frac{d}{h}\right)^{k_5}(\rho)^{k_6} \tag{32}$$

The values of the constants k_1 to k_6 are 57.292, 0.315, −0.812, −0.049, 0.678, and 0.626, where b is the corbel's width; h is the corbel's height; d is the corbel's effective height; f_y is the yield strength of longitudinal bar; f_t is the concrete tensile strength; and ρ is the longitudinal reinforcement ratio.

3.2.2. Campione Model [33]

The shear strength of fiber-reinforced concrete corbels, including stirrups, is expressed below, taking into account the influence of concrete grade, fiber volume, and reinforcement ratio:

$$V = \chi f_c{}'(bx_c \cos\alpha)\sin\alpha + \frac{b}{\sin\alpha\cos\alpha}0.2\sqrt{f_c{}'}F\left[(d - x_c)(1 - \frac{f_{ctf}}{f_y}\cdot\frac{E_s}{E_{ct}}) + c\right] \quad (33)$$

$$\chi = 0.74(\frac{f_c{}'}{105})^3 - 1.28(\frac{f_c{}'}{105})^2 + 0.22(\frac{f_c{}'}{105}) + 0.87 \quad (34)$$

$$\alpha = \frac{d - \frac{x_c}{3}}{a} \quad (35)$$

where η is the load distribution coefficient, $f_c{}'$ is the concrete tensile strength, α is the angle between the tie and strut, F is the fiber factor, f_{ctf} is the steel fiber concrete tensile strength, and c is the thickness of the protective layer.

3.2.3. Russo Model [34]

Based on the combination of the strut-and-tie mechanism resulting from cracked concrete and the main tension reinforcement, as well as the strength contribution from secondary reinforcement, the following are obtained:

$$V = 0.8(k\chi f_c{}'\cos\theta_1 + 0.65\rho_h f_{yh}\cot\theta_1)bh \quad (36)$$

$$k = \sqrt{(n\rho_f)^2 + 2n\rho_f} - n\rho_f \quad (37)$$

$$\theta = 2\arctan\left[\frac{-1 + \sqrt{(\frac{a}{d})^2 + (1 - \frac{k^2}{4})}}{\frac{a}{d} - \frac{k}{2}}\right] \quad (38)$$

$$n = \frac{42.6}{\sqrt{f_c{}'}} \quad (39)$$

where χ is the softening coefficient; θ_1 is the angle between the concrete strut and the axis of the column; and f_{yh} and ρ_h are the yield strength and reinforcement ratio of stirrup, respectively.

3.2.4. Model Validity

To validate the rationality of the proposed model in this study, the experimental results of 34 corbel tests from this study and references [35–38] were compared with the calculation results of various models proposed by researchers, including the model proposed in this study. Table 4 presents the results obtained from the study. V_{test} is the measured shear capacity values. V_n is the calculated shear capacity values by the model proposed in this study. V_F is the calculated values by the Fattuhi model. V_C is the calculated values by the Campione model. V_R is t-calculated values by the Russo model. The mean value of the test value and the Fattuhi model was 0.942, and the variance was 0.009. The calculated value of the specimen was greater than the test value, and the calculated result of the model was not safe. The mean values of the ratio calculated by the Campione model and Russo model were 1.453 and 1.311, respectively, and the variances were 0.061 and 0.017, respectively. The calculated results were conservative, and the error between the proposed model and the test value was large. From information obtained from various scholars, it can be determined that the calculation results of the proposed model are closer to the experimental values, and the variance is smaller. The shear bearing capacity of the specimen can thus be calculated accurately.

Table 4. Comparison of experimental and calculated shear bearing capital.

References	Specimens	b/mm	h_0/mm	ρ_f	V_{test}	V_{test}/V_F	V_{test}/V_C	V_{test}/V_R	V_{test}/V_n
This study	MC01	200	400	1.50%	879	0.859	1.768	1.120	1.113
	MC02	200	400	1.50%	822	1.116	1.420	1.208	1.041
	MC03	200	400	1.50%	695	1.192	1.156	1.139	1.159
	MC04	200	400	1.50%	874	0.978	1.534	1.201	1.107
	MC05	200	400	1.50%	981.5	0.929	1.750	1.270	1.114
	MC06	200	400	1.50%	670.5	0.911	1.159	1.227	1.102
	MC07	200	400	1.50%	751	1.020	1.298	1.272	1.116
	MC08	200	400	0%	775	1.018	1.342	1.148	1.144
	MC09	200	400	0.75%	767	1.071	1.321	1.130	1.173
Faleh et al. [35]	CF3-0.5	200	250	0.50%	1125	1.25	1.480	1.397	1.162
	CF3-1.0	200	250	1.00%	1220	0.960	1.435	1.356	1.104
	CF3-1.5	200	250	1.5%	1230	0.911	1.281	1.337	1.027
Fattuhi et al. [36]	1	150	125	1.70%	153	0.917	1.436	1.453	1.132
	2	150	125	1.70%	160	0.990	1.449	1.470	1.104
	3	150	129	1.70%	91.2	0.947	1.580	1.130	1.079
	4	150	127	1.70%	93	0.952	1.647	1.208	1.029
	5	150	124	1.70%	103	1.008	1.121	1.325	1.213
	6	150	125	1.70%	95.7	0.940	1.075	1.276	1.003
	9	150	125	1.70%	152.9	0.954	1.558	1.680	1.097
	10	150	124	1.70%	102.9	1.024	1.166	1.418	1.068
	12	150	127	0.70%	92	0.777	1.974	1.258	1.145
	13	150	125	1.70%	111.7	0.920	1.674	1.424	1.143
	16	150	125	1.70%	114.3	0.948	1.622	1.344	1.103
	18	150	125	1.00%	119	0.820	1.921	1.422	1.052
Yang et al. [37]	CW1	200	400	0%	1271	0.964	1.615	1.252	1.115
	CW2	200	400	0.50%	1367	1.005	1.499	1.390	1.073
	CW3	200	400	0.75%	1440	1.043	1.145	1.327	1.110
Fattuhi et al. [38]	20	153	124	1.75%	126	0.851	1.342	1.313	1.056
	21	156	122	1.50%	118	0.821	1.455	1.460	1.041
	23	153	123	2.00%	126.5	0.869	1.267	1.324	1.038
	27	153.5	124	2.50%	171.5	0.850	1.681	1.358	1.204
	32	154	120	2.00%	132.5	0.835	1.131	1.221	1.044
	39	153.5	124	2.25%	144.5	0.843	1.231	1.420	1.219
	49	154.4	122	2.50%	164.5	0.830	1.721	1.466	1.073
Mean						1.453	0.942	1.311	1.103
Variance						0.061	0.009	0.017	0.003

Figure 8 shows the comparison between the experimental values and the calculated values. In the upper left area of the figure, the experimental values are greater than the calculated values, indicating a conservative safety. The lower right area of the figure represents cases where the experimental values are smaller than the calculated values, indicating an underestimation of the safety margin. For the Fattuhi model, there is significant fluctua-

tion in the experimental data. Both the Campione model and Fattuhi model, along with their calculated results, underestimate the experimental values, indicating a conservative estimation, but with high dispersion. In contrast, the calculated values from the proposed model in this paper show a better agreement with the experimental values, with lower dispersion. This illustrates that the model proposed in this paper is more capable of accurately predicting the shear capacity of steel-fiber-reinforced high-strength concrete corbels.

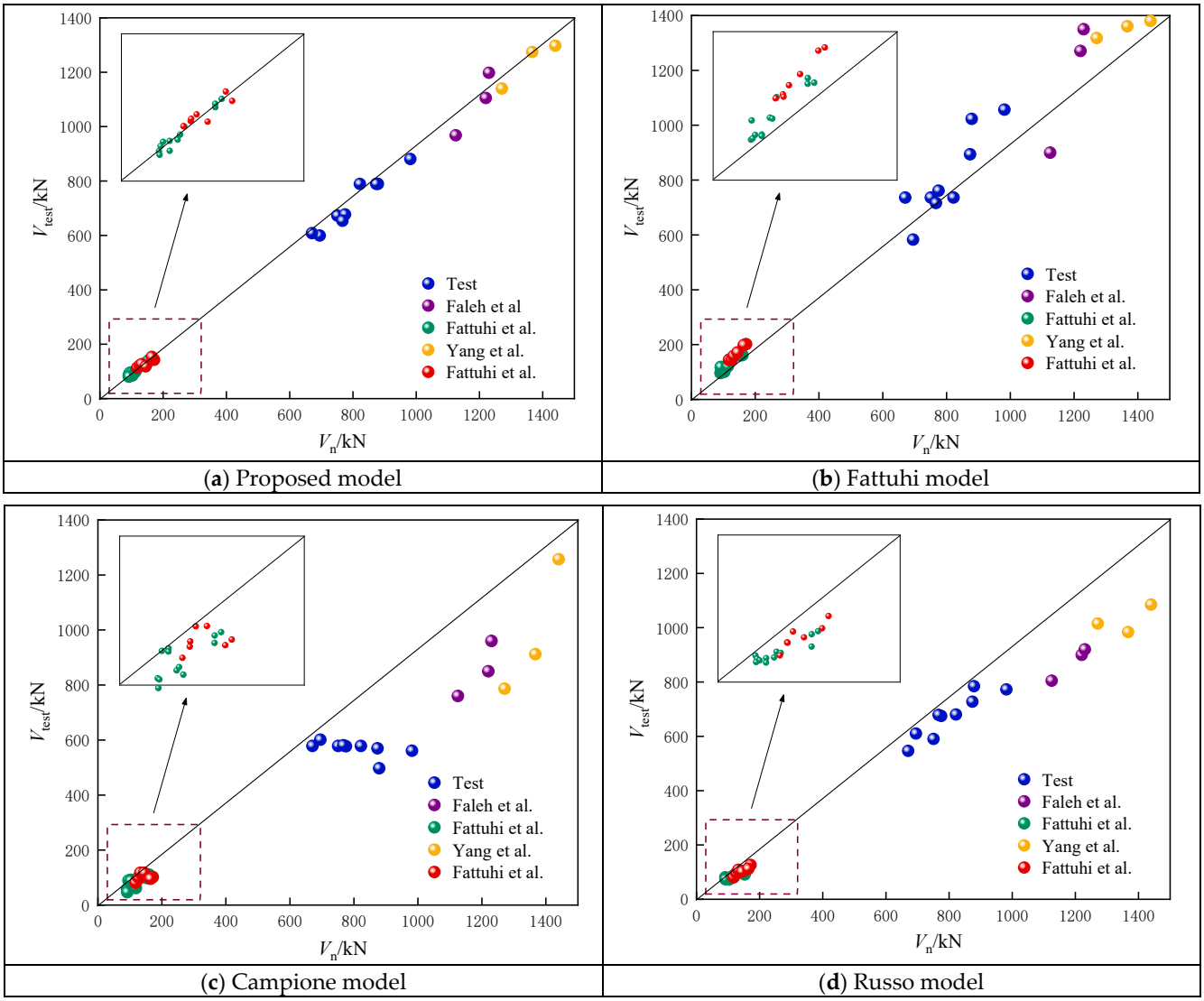


Figure 8. Comparison between test and prediction values [35–38].

4. Conclusions

This study proposes a calculation model for the shear capacity of steel-fiber-reinforced high-strength concrete corbels based on the modified compression field theory by calculating the shear capacity of 34 steel-fiber high-strength concrete corbels and comparing the results of the models proposed by various scholars. Through comparative analysis, the rationality of the proposed model is confirmed. It provides new ideas for theoretical analysis, leading to the following conclusions:

- Based on the modified compression field theory, the contribution of steel fibers to the tensile strength of concrete at crack locations is considered. The constitutive relationship of cracked steel-fiber-reinforced concrete and the local stress equilibrium equation are modified. A calculation model for the shear bearing capacity of steel-fiber-reinforced high-strength concrete corbels is proposed.

- Compared with other scholars' models, the predicted value of shear capacity calculated by the proposed model is closer to the experimental value. It can be effectively utilized for predicting and analyzing the shear bearing capacity of steel-fiber-reinforced high-strength concrete corbels, and has a clear mechanical model.

Author Contributions: Conceptualization, H.-M.L. and J.-Y.Z.; methodology, J.-Y.Z.; test, H.-M.L. and J.-Y.Z.; software, S.-S.L. and J.-Y.Z.; validation, H.-M.L. and J.-Y.Z.; formal analysis, H.-M.L. and J.-Y.Z.; investigation, H.-M.L.; resources, S.-S.L.; data curation, S.-S.L.; writing—original draft preparation, H.-M.L. and J.-Y.Z.; writing—review and editing, H.-M.L. and J.-Y.Z.; supervision, S.-S.L.; project administration, H.-M.L.; funding acquisition, S.-S.L. All authors have read and agreed to the published version of the manuscript.

Funding: This research was funded by the National Natural Science Foundation of China (No. U1404526, No. 52179133).

Data Availability Statement: Data are contained within the article.

Conflicts of Interest: The authors declare no conflicts of interest. The funders had no role in the design of the study; in the collection, analyses, or interpretation of data; in the writing of the manuscript, or in the decision to publish the results.

References

1. He, Z.Q.; Liu, Z.; Ma, Z. Investigation of Load-Transfer Mechanisms in Deep Beams and Corbels. *ACI Struct. J.* **2012**, *109*, 467–476. [CrossRef]
2. Nguyen, T.T.; Thai, H.T.; Ngo, T. Effect of steel fibers on the performance of an economical ultra-high strength concrete. *Struct. Concr. J.* **2023**, *24*, 2327–2341. [CrossRef]
3. Parthiban, P.; Kar, S.; Mondal, A.K. Stress–strain behaviour of (hpfrc) high-performance fibre reinforced concrete: An experimental study. *Mater. Today Proc.* **2023**, *80*, 3119–3123. [CrossRef]
4. Iqbal, S.; Ali, I.; Room, S. Enhanced mechanical properties of fiber reinforced concrete using closed steel fibers. *Mater. Struct. J.* **2019**, *52*, 56. [CrossRef]
5. Gali, S.; Subramaniam, K.V.L. Evaluation of crack propagation and post-cracking hinge-type behavior in the flexural response of steel fiber reinforced concrete. *Int. J. Concr. Struct. Mater.* **2017**, *11*, 365–375. [CrossRef]
6. Yun, Y.M.; Lee, Y. Strengths of Struts and Nodal Zones for Strut-and-Tie Model Design of Reinforced Concrete Corbels. *Civ. Eng. J.* **2021**, *7*, 1275–1289. [CrossRef]
7. Schlaich, J.; Schafer, K.; Jennewein, M. Toward a consistent design of reinforced concrete structures. *PCI J.* **1987**, *32*, 74–150. [CrossRef]
8. Canha, R.M.F.; Kuchma, D.A. Numerical analysis of reinforced high strength concrete corbels. *J. Eng. Struct.* **2014**, *74*, 130–144. [CrossRef]
9. Hwang, S.J.; Tsa, R.J.; Lam, W.K. Simplification of softened strut-and-tie model for strength prediction of discontinuity regions. *ACI Struct. J.* **2017**, *114*, 1569–1579. [CrossRef]
10. Abdul, R.; Khattab, S. Corbel strut and tie modeling—Experimental verification. *ACI Struct.* **2020**, *26*, 327–339. [CrossRef]
11. ACI 318 Committee. *Building Code Requirements for Structural Concrete (ACI 318-14) and Commentary*; American Concrete Institute: Farmington Hills, MI, USA, 2014.
12. Lachowicz, M.K. Experimental study of the post tensioned prestressed concrete corbels. *J. Eng. Struct.* **2016**, *108*, 1–11. [CrossRef]
13. Yang, K.H.; Ashour, A.F. Shear capacity of reinforced concrete corbels using mechanism analysis. *Struct. Build.* **2012**, *165*, 111–125. [CrossRef]
14. Wael, K. Strength Prediction of Corbels Using Strut-and-Tie Model Analysis. *Int. J. Concr. Struct. Mater.* **2015**, *9*, 255–266. [CrossRef]
15. Perceka, W.; Liao, W.C.; Wu, Y.F. Shear Strength Prediction Equations and Experimental Study of High Strength Steel Fiber-Reinforced Concrete Beams with Different Shear Span-to-Depth Ratios. *J. Appl. Sci.* **2019**, *9*, 4790. [CrossRef]
16. Jaza, H.M.; Ali, R.Y. Shear behavior of normal and high-strength concrete beams reinforced with BFRP bars and basalt macro fibers. *Constr. Build. Mater.* **2023**, *408*, 133516. [CrossRef]
17. Vecchio, F.J.; Collins, M. The modified compression field theory for reinforced concrete elements subjected to shear. *ACI Struct. J.* **1986**, *3*, 219–231. [CrossRef]
18. Kaufmann, W.; Mata, F.J.; Amin, A. Compression field analysis of fiber-reinforced concrete based on cracked membrane model. *ACI Struct. J.* **2019**, *116*, 213–224. [CrossRef]
19. Wagh, S.K.; Vianthi, A.; Liao, W.C. Experimental and MCFT-Based Study on Steel Fiber-Reinforced Concrete Subjected to In-Plane Shear Forces. *Int. J. Concr. Struct. Mater.* **2023**, *17*, 29. [CrossRef]
20. Gao, D.Y.; Shi, K. Calculation method for shear behavior of steel fiber reinforced concrete beam-column joints based on modified compression field theory. *Civ. Eng. J.* **2016**, *49*, 41–48. [CrossRef]
21. Zhang, L.Y.; Yao, J.T.; Hu, Y.K.; Gao, J. Predicting shear strength of steel fiber reinforced concrete beam-column joints by modified compression field theory. *ACI Struct. J.* **2022**, *41*, 1432–1441. [CrossRef]
22. Zhu, K.F.; Lu, J.Z.; Liu, Y.; Shao, Y.M. Shear Capacity of Hybrid Fiber Reinforced Concrete Deep Beams Based on Modified Compression Field Theory. *J. Yantai Univ.* **2016**, *29*, 216–221. [CrossRef]

23. Lei, J.; Chen, Z.X.; Shi, K.; Wang, W.G. Study on shear behavior and bearing capacity calculation of steel fiber reinforced high strength concrete two-pile caps. *J. Build. Struct.* **2023**, *44*, 234–245. [CrossRef]
24. Yan, X.; Shi, Q.X.; Xu, Z.D. Experimental study on bond behavior between concrete and deformed steel bar with different steel bar. *J. Hunan Univ.* **2020**, *47*, 45–52. [CrossRef]
25. Mortazavian, S.; Fatemi, A. Effect of fiber orientation and anisotropy on tensile strength and elastic modulus of short fiber reinforced polymer composites. *J. Compos. Part B Eng.* **2015**, *72*, 116–129. [CrossRef]
26. Huo, L.Y.; Bi, J.H.; Zhao, Y.; Wang, Z.Y. Constitutive Model of Hybrid Steel Fiber Reinforced Concrete with Different Fiber Lengths. *Constr. Build. Mater.* **2022**, *25*, 1034–1039.
27. Foster, S.J. On Behavior of High-Strength Concrete Columns: Cover Spalling, Steel Fibers and Ductility. *ACI Struct. J.* **2001**, *98*, 583–589. [CrossRef]
28. Vecchio, F.J.; Collins, M.P. Predicting the response of reinforced concrete beams subjected to subjected to shear using modified compression field theory. *ACI Struct. J.* **1988**, *85*, 258–268. [CrossRef]
29. Naaman, A.E.; Moavenzadeh, F.; Mcgarry, J. Probabilistic analysis of fiber reinforced concrete. *J. Eng. Mech. Div.* **1974**, *100*, 397–431. [CrossRef]
30. Bentz, E.C.; Vecchio, F.J.; Collins, M.P. Simplified modified compression field theory for calculating shear strength of reinforced concrete elements. *ACI Struct. J.* **2006**, *103*, 614–624. [CrossRef]
31. Collins, M.P.; Mitchell, D.; Adebar, P. A general shear design method. *ACI Struct. J.* **1996**, *93*, 36–45. [CrossRef]
32. Fattuhi, N.I. Reinforced corbels made with plain and fibrous concretes. *ACI Struct. J.* **1994**, *91*, 530–536. [CrossRef]
33. Campione, G.; Lidia, L.M.; Maria, L.M. Steel Fiber-Reinforced Concrete Corbels: Experimental Behaviour and Shear Strength Prediction. *ACI Struct. J.* **2007**, *104*, 570–579. [CrossRef]
34. Munez, P.R. Reinforced Concrete Corbels—Shear Strength Model and Design Formula. *ACI Struct. J.* **2006**, *103*, 904–906. [CrossRef]
35. Faleh, S.K.H.; Chkheiwer, A.H.; Saleh, I.S. Structural behavior of high-strength concrete corbels involving steel fibers or closed stirrups. *Period. Eng. Nat. Sci.* **2022**, *10*, 239–252. [CrossRef]
36. Fattuhi, N.I. Column-Load Effect on Reinforced Concrete Corbels. *J. Struct. Eng.* **1990**, *116*, 188–197. [CrossRef]
37. Yang, J.M.; Lee, J.H.; Yoon, Y.S. Influence of Steel Fibers and Headed Bars on the Serviceability of High-Strength Concrete Corbels. *J. Struct. Eng.* **2012**, *138*, 123–129. [CrossRef]
38. Fattuhi, N.I. Strength of SFRC Corbels Subjected to Vertical Load. *J. Struct. Eng.* **1990**, *116*, 701–718. [CrossRef]

Disclaimer/Publisher's Note: The statements, opinions and data contained in all publications are solely those of the individual author(s) and contributor(s) and not of MDPI and/or the editor(s). MDPI and/or the editor(s) disclaim responsibility for any injury to people or property resulting from any ideas, methods, instructions or products referred to in the content.